npj | 2D materials and applications

Article

Published in partnership with FCT NOVA with the support of E-MRS

https://doi.org/10.1038/s41699-024-00471-y

# CVD graphene contacts for lateral heterostructure MoS2 field effect transistors



Daniel S. Schneider[1,2], Leonardo Lucchesi[3], Eros Reato[1,2], Zhenyu Wang[4], Agata Piacentini[1,2], Jens Bolten[1], Damiano Marian[3], Enrique G. Marin[5], Aleksandra Radenovic[4], Zhenxing Wang[1], Gianluca Fiori[3], Andras Kis[4], Giuseppe Iannaccone[3], Daniel Neumaier[1,6] & Max C. Lemme[1,2] ✉

Intensive research has been carried out on two-dimensional materials, in particular molybdenum disulfide, towards high-performance field effect transistors for integrated circuits[1]. Fabricating transistors with ohmic contacts is a challenging task due to the formation of a high Schottky barrier that severely limits the performance of the transistors for real-world applications. Graphene-based heterostructures can be used in addition to, or as a substitute for unsuitable metals. In this paper, we present lateral heterostructure transistors made of scalable chemical vapor-deposited molybdenum disulfide and chemical vapor-deposited graphene achieving a low contact resistances of about 9 kΩ·µm and high on/off current ratios of $10^8$. Furthermore, we also present a theoretical model calibrated on our experiments showing further potential for scaling transistors and contact areas into the few nanometers range and the possibility of a substantial performance enhancement by means of layer optimizations that would make transistors promising for use in future logic integrated circuits.

Two-dimensional (2D) semiconducting materials from the group of transition metal dichalcogenides (TMDCs) are promising for aggressively scaled transistors for next-generation integrated circuits that are largely unaffected by short-channel effects[2–5]. By now, stable wafer-based deposition techniques have been achieved for the most studied TMDC molybdenum disulfide ($MoS_2$)[6–9]. Also, $MoS_2$ has been demonstrated as a suitable channel material for n-type field-effect transistors (FETs) with high performance[10–12] and has been successfully used in circuits[13–15]. Low-voltage and low-power applications require transistors that not only exhibit sufficiently high mobility and high current on/off ratio but also low contact resistance between the metal electrodes and the 2D channel. Direct contacting of $MoS_2$ with metals can lead to the formation of Schottky barriers and Fermi-level pinning at the interfaces. The results are undesirably high contact resistances and therefore limited carrier injection and, ultimately, reduced device performance[16,17]. For this reason, various contact methods were evaluated. The use of $MoS_2$ phase-transformed from semiconducting 2H into metallic 1 T has been proposed as a contact region[18]. However, it should be noted that stable 1 T contact regions have not yet been reproducibly demonstrated with chemical vapor deposited (CVD)-grown $MoS_2$. Others have demonstrated that ultra-high vacuum-deposited Au contacts can also lead to very low contact resistance[12,19,20]. However, gold is typically not suitable for monolithic integration due to the lack of silicon CMOS compatibility. A further approach is chloride molecular doping, which leads to a significant reduction of contact resistance but is also unstable over time[21]. Recently, McLellan et al.[22] presented a stable doping process that can lead to very low contact resistance through aluminum oxide ($AlO_x$) capping, but also induces strong n-doping and cannot easily be limited to the contact regions[22]. Another approach to achieving very low contact resistances to 2D materials is to use semimetals like bismuth and antimony[23,24], although they are relatively scarce, which may limit their long-term use as contact metals[25]. Graphene, on the other hand, has excellent electrical conductivity and is chemically stable, making it a promising candidate for low-resistance contacts to $MoS_2$[26–34]. Several reports have already proven the versatility of graphene as a contact due to the tunability of its work function by electrostatic doping, which minimizes the Schottky barrier height at the graphene-semiconductor interface[26,32,35–37]. Using the semimetal graphene as contacts provides an atomically sharp interface without dangling bonds, so the Fermi-level pinning[38] at the contact interface to TMDCs can be prevented[33]. The mechanical strength, flexibility, transparency, and thermal stability of 2D materials make them highly desirable for flexible electronics

[1]Advanced Microelectronic Center Aachen (AMICA), AMO GmbH, Aachen, Germany. [2]RWTH Aachen University, Aachen, Germany. [3]University of Pisa, Pisa, Italy. [4]École Polytechnique Fédérale de Lausanne (EPFL), Lausanne, Switzerland. [5]University of Granada, Granada, Spain. [6]University of Wuppertal, Wuppertal, Germany. ✉e-mail: lemme@amo.de

applications[39]. Here, device bendability is a significant concern. Graphene contacts can offer an excellent alternative to traditional metals, which are often the limiting factor in high strain levels. Although the advantages of graphene are apparent, the graphene sheet resistance and the metal-graphene contact resistance contribute to the total resistance in addition to the graphene-TMDC contact resistance and, therefore, must be co-optimized in the contact design and fabrication. Furthermore, the employment of graphene contacts required an additional metallization layer for electrical characterization due to the inherent thinness of graphene as an electrode. An intrinsic limitation of these contacts is the high van der Waals gap, which is, in some cases, higher than the metal-$MoS_2$ gap[40]. This issue can, however, be addressed by achieving a perfect edge contact between the metal and the graphene[41].

In this work, we experimentally demonstrate a scalable technique for low contact resistance to $MoS_2$ using CVD-grown SLG. We further show that metal one-dimensional edge contacts between single-layer graphene (SLG) and nickel (Ni) are a suitable method for achieving low contact resistances[42,43]. The results are corroborated through simulations that explore the scalability potential of further contact resistance optimization based on this approach.

## Results

### Material characterization

Confocal Raman measurements were performed on the SLG/$MoS_2$ lateral heterostructure (LH) (Fig. 1a) to analyze the transferred 2D films. A Raman map with 400 points taken after the transfer of SLG on $SiO_2$ in Fig. 1b shows the 2D (2692 $cm^{-1}$) and G (1589 $cm^{-1}$) modes of SLG. A defect peak around 1350 $cm^{-1}$ was not detected, indicating high-quality graphene after the transfer. The thickness of $MoS_2$, as measured by atomic force microscopy in a prior growth process, is approximately 0.7 nm and aligns with the Raman data confirming its monolayer structure[9].

A spatially resolved Raman map of a µm-scale FET was performed (red box in Fig. 1c). The strong intensity of the $A_{1g}$ mode of $MoS_2$ in Fig. 1d confirms that the $MoS_2$ channel uniformly covers the entire region between the Ni contacts, while SLG is in contact with the Ni and the $MoS_2$.

### Device characteristics

The contact resistance $R_c$ of Ni edge contacts to SLG is typically in the range of only a few hundred Ω µm and the sheet resistance $R_s$ of SLG is ~1 kΩ/square[43] (Supplementary Fig. 4), more than 100x lower than that of $MoS_2$.

Figure 2a shows the transfer characteristic for $V_{ds}$ = 1 V with measured maximum on current of $I_{on}/W$ = 43 µA/µm for a device with $L_{ch}$ = 100 nm and $V_{gs}$ = 40 V.

The transfer characteristics of a LH-FET with $L_{ch}$ = 1 µm is shown in Fig. 2b. This device reached a high current on/off ratio of more than $10^8$ with a low off-current of order 10 fA/µm at $V_{gs}$ = −30 V (a graph with a wider $V_{gs}$ sweep is shown in Supplementary Fig. 3). The transfer curves show a kink at $V_{gs}$ = −20 V, which can be attributed to acceptor-like interface states in S/D regions[44]. The output curves of the 1 µm-long LH-FET in Fig. 2c demonstrate an ohmic behavior of the drain currents, indicating the suitable contacting scheme with graphene. The drain current's saturation range is limited by the relatively thick gate oxide (90 nm $SiO_2$), which hinders the build-up of a strong electrostatic potential across the channel. The on-currents of the device increase continuously as the channel length decreases with approximately a $1/\sqrt{L_{ch}}$ relationship, as shown in Fig. 3a for $V_{ds}$ = 100 mV (red) and $V_{ds}$ = 1 V (black) at $V_{gs}$ = 40 V. The transmission line method (TLM) was used to extract a contact resistance from the total resistance

$$R_{total} = 2 \cdot R_c + R_{ch} \quad (1)$$

where $R_{ch}$ is the channel resistance. Figure 3b shows the linear fit of $R_{total}$ for different $L_{ch}$, and the point at which the line intersects the Y-axis corresponds to a value of 2·$R_c$. Here, a $R_c = 9 \pm 2$ kΩ µm was extracted for the LH-FET, which is more than one order of magnitude lower than reference $MoS_2$ FETs with pure Ni side contacts (Supplementary Fig. 5 and a

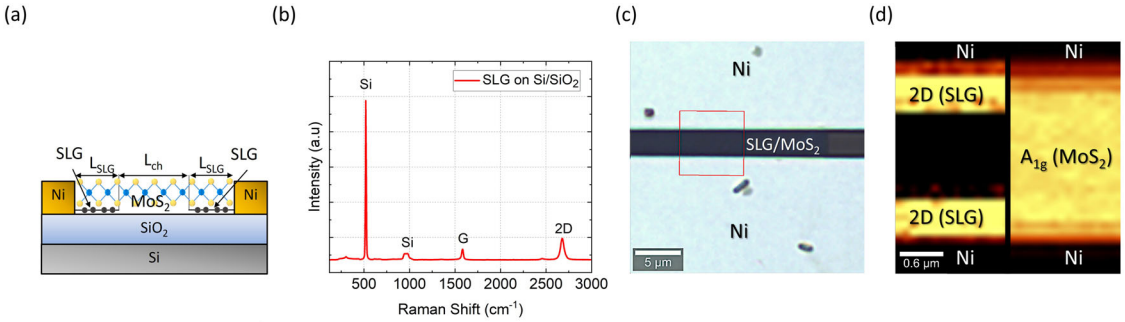


**Fig. 1 | Overview of the sample design and 2D-layers arrangement. a** Device schematic of LH-FETs. $L_{SLG}$ describes the length of the SLG/$MoS_2$ heterostructure and $L_{ch}$ defines the channel of the transistor. **b** Raman spectrum of SLG on Si/$SiO_2$ before the transfer of MoS2. **c** Optical microscope image of a LH-FET. The Raman area scan shown in **d** was performed in the area marked by the red box. **d** A spatially resolved Raman map shows the intensity of the 2D mode of SLG (left) and the intensity of the $A_{1g}$ mode of $MoS_2$ (right). Dark areas indicate not present mode while brighter areas indicate a stronger intensity.

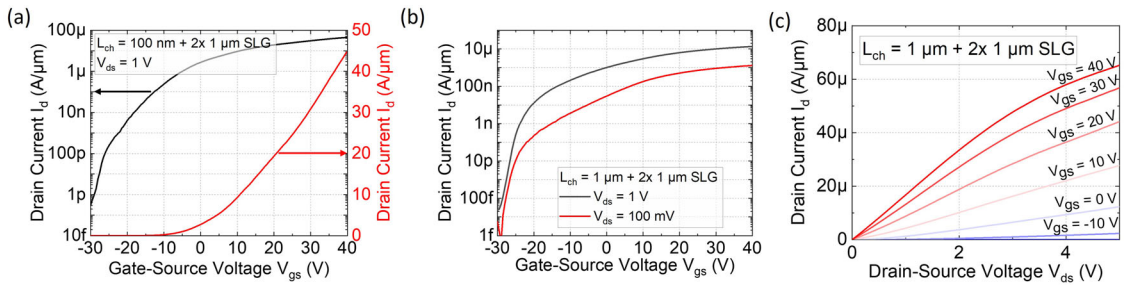


**Fig. 2 | Transistor performance characteristics of the devices. a** Transfer characteristic of a $MoS_2$ LH-FET with $L_{ch}$ = 100 nm for $V_{ds}$ = 1 V in log scale (black line) and linear scale (red line). **b** Transfer characteristic of a LH-FET with $L_{ch}$ = 1 µm for $V_{ds}$ = 1 V (black line) and $V_{ds}$ = 100 mV (red line) and (**c**) its corresponding output curves.

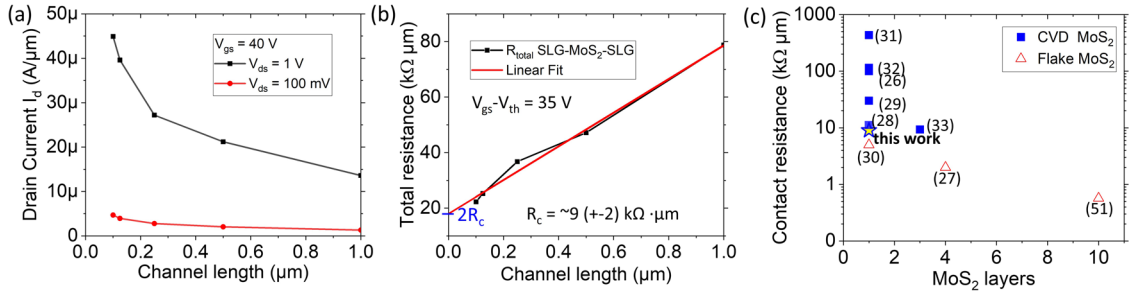


**Fig. 3 | Additional performance data and benchmarking of the contact resistances. a** Ion is plotted against $L_{ch}$ for $V_{ds}$ = 1 V (black line) and $V_{ds}$ = 100 mV (red line) in double-logarithmic scale. **b** Total device resistance vs channel length of different LH-FETs and the extracted contact resistance by TLM. **c** Benchmarking plot of contact resistance of graphene-contacted $MoS_2$ FETs[26–30,32,33,51] as a function of $MoS_2$ layers (blue: CVD $MoS_2$; red: exfoliated $MoS_2$).

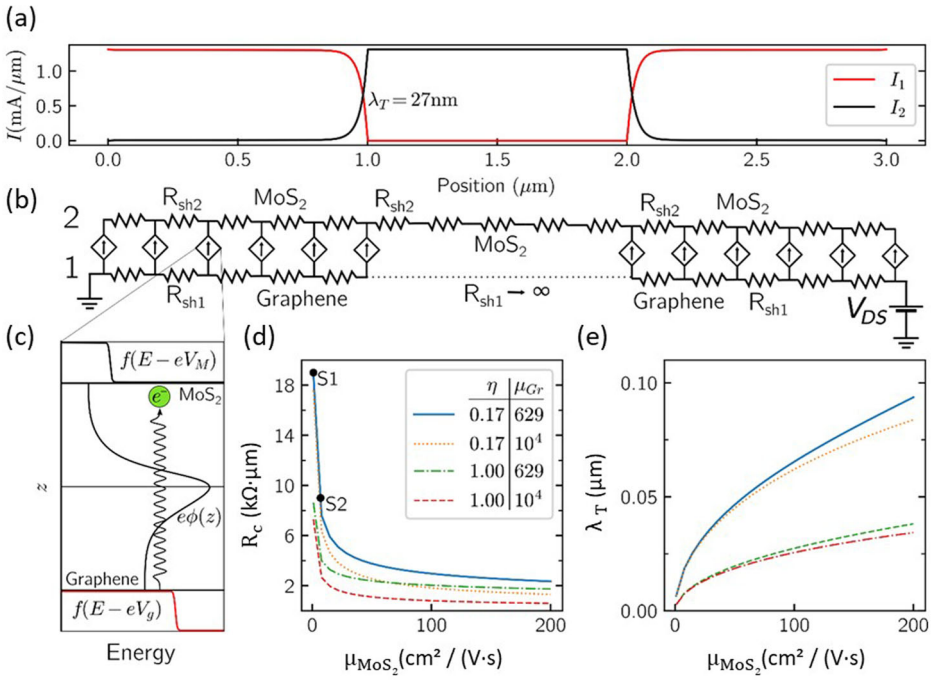


**Fig. 4 | Multiscale simulation of transport.** **a** Simulated horizontal current for each layer in the whole device for typical device operation conditions. Horizontal current transfer between the graphene layer (1) and the $MoS_2$ layer (2) shows the presence of vertical carrier transport over a few transfer lengths $\lambda_T$. **b** Circuit-like schematization of the device, a non-linear Transmission Line Model setup. Vertical ballistic transport between the two resistive layers is represented by nonlinear current generators. **c** Depiction of vertical ballistic transport. Carriers propagate through the interlayer barrier $\phi(z)$ from the local Fermi distributions generated by local electrostatic potentials $V_{1,2}(x)$. **d** Simulated dependence of contact resistance $R_c$ on $MoS_2$ mobility $\mu_{(MoS\_2)}$ for different interface quality $\eta$ and graphene mobility $\mu_{Gr}$. Our simulation correctly predicts the difference in contact resistance between two samples (S1 and S2) with different $\mu_{(MoS\_2)}$. **e** Simulated transmission length $\lambda_T$ dependence on $\mu_{(MoS\_2)}$ for different $\eta$ and $\mu_{Gr}$ (same legend as **d**). $\lambda_T$ does not depend strongly on $\mu_{Gr}$.

comparison of transfer characteristics of LH-FETs and Ni contacted FETs in Supplementary Fig. 6). For both types of devices, a sheet resistance of $R_s \sim 60$ kΩ/square was extracted. To demonstrate the scalability of our approach, we conducted measurements on 10 LH-FETs for each channel length (Supplementary Fig. 8), revealing minimal device-to-device variability. A benchmarking plot of literature data compares contact resistances of multilayer CVD and exfoliated $MoS_2$ FETs contacted with graphene (Fig. 3c). The comparison has been made among graphene-contacted $MoS_2$-FETs to emphasize the importance of this scalable approach, which still has a margin of improvement in the quality of the materials. Even though flake-based $MoS_2$ and graphene have previously achieved lower contact resistances, this work stands out by utilizing scalable materials and demonstrating the lowest reported contact resistance on a CVD monolayer $MoS_2$ channel, narrowing the gap with the superiority with flakes-based materials.

## Device simulation

To better understand device operation and the potential of downscaling to nanometer size, we performed a multiscale simulation of the LH-FET.

In our model, we describe the top contact as a ladder of resistors and current generators, as shown in Fig. 4a. The horizontal (in-plane) resistors have a resistance proportional to the layers' sheet resistances and the vertical current generators provide the vertical current per unit area due to ballistic transport, which is nonlinearly dependent on the electrochemical potentials of the two nodes and on the vertical electrostatic potential profile. Since we can define local electrochemical potentials for each layer $\mu_{Gr}(x)$ and $\mu_{MoS_2}(x)$ on the horizontal direction, the nonlinear current generators are described through a modified Landauer formula where, in order to use measurable quantities, we use the in-layer applied potentials defined as

$$V_i(x) = -(1/e)\mu_i(x) \tag{2}$$

instead of the chemical potentials:

$$I_v(x) = I_0 \cdot \int T\left(E, \phi\left(V_{Gr}(x), V_{MoS_2}(x)\right)\right) \left(f\left(E + V_{MoS_2}(x)\right) - f\left(E + V_{Gr}(x)\right)\right) dE \tag{3}$$

Assuming that the electrostatic potential varies smoothly in the horizontal direction, we can compute the electrostatic potential for every horizontal position $x$ through a vertical 1D Poisson simulation dependent the on the gate voltage $V_{gs}$ and the applied potentials. In general, the interlayer transmission coefficient $T(E, x)$ depends on the detailed shape of the

electrostatic potential in the vertical direction. Assuming that the difference between the electrochemical potential of the two layers is small, we can approximate $T(E,x)$ as a $T(E+e\phi(x))$, where $\phi(x)$ is the average of the electrostatic potentials of the two layers for the same horizontal coordinate x:

$$\phi(x) = (\phi_{Gr}(x) + \phi_{MoS_2}(x))/2 \tag{4}$$

This corresponds to considering that the shape of the barrier in the vertical direction is negligibly dependent on the electrochemical potential of the layers and that the transmission coefficient in the vertical direction is only affected by the average shift of the barrier. We computed $T(E)$ through a multiscale approach considering two infinite layers at equilibrium following the procedure described in the methods section.

The solution of the Poisson equations enables us at the same time to use the aforementioned approximation to shift $T(E)$ to $T\big(E+e\phi(x)\big)$, and to compute the carrier densities in the two layers, which in turn affect the sheet resistances

$$R_{sh,a}(x) = \frac{1}{\left[e\mu_{c,a}n_{s,a}(x)\right]} \tag{5}$$

where $n_{s,a}(x)$ is the majority carrier density and $\mu_c$ is the carrier mobility in the layer denoted by $a$, where $(a = Gr, \mathrm{MoS_2})$.

The effect of the gate voltage $V_{gs}$ is therefore entirely embodied in $T(E+\phi(x))$ and $R_{sh,1,2}(x)$. The model parameters are the materials' mobilities $\mu_{c,Gr}$, $\mu_{c,MoS2}$, and the corresponding doping densities $n_{Gr}$, $n_{MoS_2}$. We estimated $n_{Gr}$ on the $SiO_2$ substrate to be $4.5\times10^{12}\mathrm{cm}^{-2}$ from the position of the charge neutral point in an analogous structure in ref. 43, while for the $MoS_2$ we assume it to be $2\times10^{12}cm^{-2}$. Using the estimated doping densities, we could use carrier densities obtained from Poisson simulations to estimate $\mu_{c,Gr}$ and $\mu_{c,MoS2}$ respectively from the sheet resistance of ref. 43 and the channel sheet resistance obtained from the TLM depicted in Supplementary Fig. 7 by inverting

$$R_{sh} = \frac{1}{\left[e\mu_c n_s\right]} \tag{6}$$

for $MoS_2$ we estimated it to be $\mu_{c,MoS2}\approx 1\mathrm{cm}^2\mathrm{V}^{-1}\mathrm{s}^{-1}$ for sample 1 and $\mu_{c,MoS2}\approx7\mathrm{cm}^2\mathrm{V}^{-1}\mathrm{s}^{-1}$ for sample 2, and for graphene we estimated it to be $\mu_{c,Gr2}\approx 629\mathrm{cm}^2\mathrm{V}^{-1}\mathrm{s}^{-1}$. We also introduced a single fitting parameter: the interface quality factor $\eta$, defined as

$$\eta = \frac{I_0}{I_{0,Landauer}} \tag{7}$$

which represents the missing knowledge on the actual distance between the planes and the overall interface quality.

We cast our model in a non-linear transmission line model structure, where we solved a system of differential equations describing horizontal transport with source terms representing vertical transport[43]. Our model allowed us to obtain the applied potentials $V_{Gr,MoS_2}(x)$ and the horizontal currents $I_{Gr,MoS_2}(x)$ profiles in the two layers. From these current profiles, we could extract two main quantities describing the performance of the top contact (i) contact resistance ($R_c$) and (ii) transfer length ($\lambda_T$). The former is the main figure of merit of a contact. With our calculation we confirm the experimental result by obtaining $R_c = 9k\Omega\cdot\mu m$ for the estimated mobility of sample 2. As for the latter, which represents the characteristic length over which the current goes from one layer to the other, and therefore the minimum length for the top contact, we obtain $\lambda_T = 27nm$, showing potential for contact length scaling and integration. Low resistance is achieved by inserting the semimetal graphene between the metal and the 2D semiconductor. As demonstrated in Shen et al.[23], this partially avoids the formation of the hybridized states in the gap of the semiconductor that lead to the Fermi pinning phenomenon. The relatively low Schottky barrier between graphene and $MoS_2$ of $\sim0.5$ eV can be further reduced electrostatically via the gate voltage, since graphene is a semimetal, and we cannot assume it to have an infinite density of states[26,35,36,45]. Furthermore, the gate voltage introduces a large carrier density in the contact, further improving conductivity. The use of an advanced fabrication process also ensures a clean heterostructure with a low density of impurities and defects.

The main confirmation of the validity of our model is the correct scaling of contact resistance $R_c$ with $\mu_{c,MoS2}$. As we can see in Fig. 4d, by increasing $\mu_{c,MoS2}$ while keeping every other parameter constant implies a nonlinear decrease in $R_c$. Our mobility scaling can describe $R_c$ in two samples with different mobilities by using the same value for $\eta$. This suggests that $\eta$ is a general parameter, depending only on materials choice and interface quality, not on the quality of the materials. Therefore, obtaining the value of $\eta$ for one value of $\mu_{c,MoS2}$ allowed us to extrapolate the contact resistance for contacts made with higher quality materials, assessing the potential of the Ni-graphene/$MoS_2$ contact for future practical applications. We can see that even if the contact would have been made of materials with record mobilities ($\sim10000\ \mathrm{cm}^2\mathrm{V}^{-1}\mathrm{s}^{-1}$) for graphene[44] and $\sim200\ \mathrm{cm}^2\mathrm{V}^{-1}\mathrm{s}^{-1}$ for $MoS_2$[10]), with the current interface quality $\eta = 0.17$ the minimum contact resistance would have been $R_c\sim2k\Omega\cdot\mu m$ with a transfer length of $\lambda_T\sim80nm$. For an ideal interface quality $\eta = 1$, we can estimate the minimum achievable contact resistance to be $R_c\sim0.5k\Omega\cdot\mu m$ with $\lambda_T\sim35nm$. Figure 4d also shows that interface quality is even more important than the 2D-materials mobilities since the contact resistance quickly saturates because of the effective resistance of the vertical interface.

In summary, we have experimentally demonstrated lateral SLG/$MoS_2$ heterostructures based on scalable materials, with low contact resistances down to ~9 kΩ μm at current ON/OFF ratios of $10^8$. The proposed theoretical model, calibrated with experiments, shows a charge transfer length down to 27 nm, indicating the scaling potential of the SLG approach for ultra-scaled 2D FETs. Furthermore, our model shows that TMDCs with higher mobility and an optimized interface can lead to a very promising contact resistance of 0.5 kΩ μm. Here, direct growth processes or cleaner transfers of large area grown 2D materials are necessary to improve the interfaces of heterostructures and thus lower contact resistance in future scalable devices.

## Methods

### $MoS_2$ deposition

A continuous single-layer $MoS_2$ film was grown by metal-organic chemical vapor deposition (MOCVD) on 2" sapphire wafer using molybdenum hexacarbonyl ($Mo(CO)_6$) and hydrogen disulfide ($H_2S$) precursors[9]. Extensive characterization of the material has been performed in reference[9]., including transmission electron microscopy (TEM) to assess the quality of the material.

### Material characterization

Confocal Raman and PL measurements were performed with a laser wavelength of 532 nm and a power of 1 mW on $MoS_2$ in detail, both on its growth substrate sapphire and after being transferred onto 90 nm silicon oxide on silicon substrates (Supplementary Fig. 1). PL measurements of $MoS_2$ and Raman measurements of SLG were conducted with a 300 lines/mm grating and Raman measurements of $MoS_2$ with a 1800 lines/mm grating. The step height of ~0.7 nm of $MoS_2$ was measured by atomic force microscopy.

### Device fabrication

Commercially available CVD grown SLG on copper (Cu) was transferred onto a 90 nm $SiO_2$/Si substrate with pre-patterned alignment marker via PMMA supported wet transfer. Electron beam lithography (EBL) and Oxygen ($O_2$) plasma reactive ion etching (RIE) were used to pattern the SLG contact areas. CVD-$MoS_2$ was then transferred onto the entire chip by wet transfer[46]. FET channels were defined by EBL and subsequent RIE using a gas mixture of tetrafluoromethane ($CF_4$) and $O_2$. Finally, self-aligned sputtered Ni edge contacts to SLG were defined by EBL and a subsequent

$CF_4/O_2$ plasma RIE process using the same resist mask. The back-gated FETs with different channel lengths from 100 nm to 1 µm were used to determine the contact resistance by Transfer-Line-Method (TLM). The relatively large device channel width of 100 µm was used to compensate single material defects in the 2D layers or residues caused by the transfers[47]. A sketch of the fabrication process of lateral heterostructure (LH)-FETs is shown in Figure S2. Although graphene and $MoS_2$ are vertically stacked, the term 'lateral heterostructure 'refers to the lateral transistor configuration wherein the $MoS_2$ channel can be modulated between two graphene contacts.

### Computational methods

The device model required a correct description of the physics and the two largely different length scales in the horizontal direction ( ~ 1 µm) and in the vertical direction ( ~ 1 nm). For this reason, we assume diffusive transport in the horizontal direction and ballistic transport in the vertical direction across the van-der-Waals gap of the heterojunction. These two very different transport regimes were described with a single multiscale model. As for the ballistic transport, we compute the vertical transmission coefficient between graphene and $MoS_2$ following the procedure detailed in ref. 48, which consists in performing (i) a density functional theory (DFT) simulations of the infinite graphene-$MoS_2$ heterostructure, (ii) a transformation of the DFT Hamiltonian into the basis of maximally localized Wannier function (MLWF) using proper projection in order to clearly identify the top and bottom flake, i.e., $MoS_2$ and graphene, (iii) non-equilibrium Green's function (NEGF) simulation to compute the vertical transmission, creating a proper MLWF Hamiltonian with monolayer and bilayer regions[48]. DFT calculations have been carried out using Quantum Espresso suite[49]. We have considered a supercell consisting of $4 \times 4$ graphene and $3 \times 3$ $MoS_2$ elementary cells, applying 3% of strain on the graphene and no strain on $MoS_2$, with an interlayer distance of 3.4 A. We use GGA-PBE pseudopotentials and grimme-D2 correction to consider van der Waals forces. Calculations are performed on a $3 \times 3 \times 1$ grid. The Hamiltonian in terms of the MLWF has been obtained exploiting Wannier90 code[50] projecting on the $p_z$ orbital of each C atom and on the three *sp2* orbitals every two C atoms while on the *d*-orbitals for the Mo and on the *s*- and the *p*-orbitals for the S atoms. The transmission coefficient has been obtained using NanoTCAD ViDES (NanoTCAD ViDES.).

## Data availability

Data sets generated during the current study are available from the corresponding authors upon reasonable request.

Received: 3 April 2023; Accepted: 15 April 2024;
Published online: 10 May 2024

## References

1. Tosun, M. et al. High-gain inverters based on $WSe_2$ complementary field-effect transistors. *ACS Nano* **8**, 4948–4953 (2014).
2. Yoon, Y., Ganapathi, K. & Salahuddin, S. How good can monolayer MoS2 transistors be? *Nano Lett.* **11**, 3768–3773 (2011).
3. Sebastian, A., Pendurthi, R., Choudhury, T. H., Redwing, J. M. & Das, S. Benchmarking monolayer MoS 2 and WS 2 field-effect transistors. *Nat. Commun.* **12**, 693 (2021).
4. Chung, Y.-Y. et al. First Demonstration of GAA Monolayer-MoS2 Nanosheet nFET with 410µA/µm ID at 1V VD at 40nm gate length. in *2022 International Electron Devices Meeting (IEDM)* 34.5.1–34.5.4 https://doi.org/10.1109/IEDM45625.2022.10019563 (2022).
5. Lemme, M. C., Akinwande, D., Huyghebaert, C. & Stampfer, C. 2D materials for future heterogeneous electronics. *Nat. Commun.* **13**, 1392 (2022).
6. Kang, K. et al. High-mobility three-atom-thick semiconducting films with wafer-scale homogeneity. *Nature* **520**, 656–660 (2015).
7. Yu, H. et al. Wafer-scale growth and transfer of highly-oriented monolayer MoS2 continuous films. *ACS Nano* **11**, 12001–12007 (2017).
8. Marx, M. et al. Metalorganic vapor-phase epitaxy growth parameters for two-dimensional MoS2. *J. Electron. Mater.* **47**, 910–916 (2018).
9. Cun, H. et al. Wafer-scale MOCVD growth of monolayer MoS2 on sapphire and SiO2. *Nano Res.* **12**, 2646–2652 (2019).
10. Radisavljevic, B., Radenovic, A., Brivio, J., Giacometti, V. & Kis, A. Single-layer MoS2 transistors. *Nat. Nanotechnol.* **6**, 147–150 (2011).
11. Smets, Q. et al. Ultra-scaled MOCVD MoS2 MOSFETs with 42nm contact pitch and 250µA/µm drain current. in *2019 IEEE International Electron Devices Meeting (IEDM)* 23.2.1–23.2.4 https://doi.org/10.1109/IEDM19573.2019.8993650 (2019).
12. Chou, A.-S. et al. High on-state current in chemical vapor deposited monolayer MoS2 nFETs with Sn ohmic contacts. *IEEE Electron Device Lett.* **42**, 272–275 (2021).
13. Radisavljevic, B., Whitwick, M. B. & Kis, A. Integrated circuits and logic operations based on single-layer MoS2. *ACS Nano* **5**, 9934–9938 (2011).
14. Polyushkin, D. K. et al. Analogue two-dimensional semiconductor electronics. *Nat. Electron.* **3**, 486–491 (2020).
15. Conti, S. et al. Low-voltage 2D materials-based printed field-effect transistors for integrated digital and analog electronics on paper. *Nat. Commun.* **11**, 3566 (2020).
16. Liu, W., Sarkar, D., Kang, J., Cao, W. & Banerjee, K. Impact of contact on the operation and performance of back-gated monolayer MoS2 field-effect-transistors. *ACS Nano* **9**, 7904–7912 (2015).
17. Schulman, D. S., Arnold, A. J. & Das, S. Contact engineering for 2D materials and devices. *Chem. Soc. Rev.* **47**, 3037–3058 (2018).
18. Kappera, R. et al. Phase-engineered low-resistance contacts for ultrathin MoS2 transistors. *Nat. Mater.* **13**, 1128–1134 (2014).
19. English, C. D., Shine, G., Dorgan, V. E., Saraswat, K. C. & Pop, E. Improved contacts to MoS2 transistors by ultra-high vacuum metal deposition. *Nano Lett.* **16**, 3824–3830 (2016).
20. Smithe, K. K. H., English, C. D., Suryavanshi, S. V. & Pop, E. High-field transport and velocity saturation in synthetic monolayer $MoS_2$. *Nano Lett.* **18**, 4516–4522 (2018).
21. Yang, L. et al. Chloride molecular doping technique on 2D materials: $WS_2$ and $MoS_2$. *Nano Lett.* **14**, 6275–6280 (2014).
22. McClellan, C. J., Yalon, E., Smithe, K. K. H., Suryavanshi, S. V. & Pop, E. High current density in monolayer MoS2 doped by AlOx. *ACS Nano* **15**, 1587–1596 (2021).
23. Shen, P.-C. et al. Ultralow contact resistance between semimetal and monolayer semiconductors. *Nature* **593**, 211–217 (2021).
24. Li, W. et al. Approaching the quantum limit in two-dimensional semiconductor contacts. *Nature* **613**, 274–279 (2023).
25. Henckens, T. Scarce mineral resources: Extraction, consumption and limits of sustainability. *Resour. Conserv. Recycling* **169**, 105511 (2021).
26. Yu, L. et al. Graphene/MoS2 Hybrid Technology for Large-Scale Two-Dimensional Electronics. *Nano Lett.* **14**, 3055–3063 (2014).
27. Cui, X. et al. Multi-terminal transport measurements of MoS 2 using a van der Waals heterostructure device platform. *Nat. Nanotechnol.* **10**, 534–540 (2015).
28. Zhao, M. et al. Large-scale chemical assembly of atomically thin transistors and circuits. *Nat. Nanotechnol.* **11**, 954–959 (2016).
29. Guimarães, M. H. D. et al. Atomically thin ohmic edge contacts between two-dimensional materials. *ACS Nano* **10**, 6392–6399 (2016).
30. Xie, L. et al. Graphene-contacted ultrashort channel monolayer MoS2 transistors. *Adv. Mater.* **29**, 1702522 (2017).
31. Hong, W., Shim, G. W., Yang, S. Y., Jung, D. Y. & Choi, S.-Y. Improved Electrical Contact Properties of $MoS_2$-Graphene Lateral Heterostructure. *Adv. Funct. Mater.* **29**, 1807550 (2019).
32. Chee, S.-S. et al. Lowering the Schottky Barrier Height by Graphene/Ag Electrodes for High-Mobility MoS2 Field-Effect Transistors. *Adv. Mater.* **31**, 1804422 (2019).

33. Mootheri, V. et al. Graphene based Van der Waals contacts on $MoS_2$ field effect transistors. *2D Mater.* **8**, 015003 (2020).
34. Tang, J. et al. Vertical Integration of 2D Building Blocks for All-2D Electronics. *Adv. Electron. Mater.* **6**, 2000550 (2020).
35. Qiu, D. & Kim, E. K. Electrically Tunable and Negative Schottky Barriers in Multi-layered Graphene/MoS2 Heterostructured Transistors. *Sci. Rep.* **5**, 13743 (2015).
36. Du, H. et al. Schottky barrier contrasts in single and bi-layer graphene contacts for MoS2 field-effect transistors. *Appl. Phys. Lett.* **107**, 233106 (2015).
37. Jin, C., Rasmussen, F. A. & Thygesen, K. S. Tuning the Schottky barrier at the graphene/MoS2 interface by electron doping: density functional theory and many-body calculations. *J. Phys. Chem. C* **119**, 19928–19933 (2015).
38. Kim, C. et al. Fermi level pinning at electrical metal contacts of monolayer molybdenum dichalcogenides. *ACS Nano* **11**, 1588–1596 (2017).
39. Akinwande, D. et al. A review on mechanics and mechanical properties of 2D materials—Graphene and beyond. *Extrem. Mech. Lett.* **13**, 42–77 (2017).
40. Ma, Y., Dai, Y., Guo, M., Niu, C. & Huang, B. Graphene adhesion on MoS2 monolayer: an ab initio study. *Nanoscale* **3**, 3883–3887 (2011).
41. Allain, A., Kang, J., Banerjee, K. & Kis, A. Electrical contacts to two-dimensional semiconductors. *Nat. Mater.* **14**, 1195–1205 (2015).
42. Wang, L. et al. One-dimensional electrical contact to a two-dimensional material. *Science* **342**, 614–617 (2013).
43. Shaygan, M. et al. Low resistive edge contacts to CVD-grown graphene using a CMOS compatible metal. *Ann. der Phys.* **529**, 1600410 (2017).
44. Rodder, M. A. & Dodabalapur, A. Phenomenological model of gate-dependent kink in I-V characteristics of MoS2 double-Gate FETs. *IEEE. J. Electron Devices Soc.* **9**, 441–446 (2021).
45. Chuang, H.-J. et al. High mobility WSe2 p- and n-type field-effect transistors contacted by highly doped graphene for low-resistance contacts. *Nano Lett.* **14**, 3594–3601 (2014).
46. Schneider, D. S. et al. Highly responsive flexible photodetectors based on MOVPE grown uniform few-layer MoS2. *ACS Photonics* **7**, 1388–1395 (2020).
47. Tongay, S. et al. Tuning interlayer coupling in large-area heterostructures with CVD-grown MoS2 and WS2 monolayers. *Nano Lett.* **14**, 3185–3190 (2014).
48. Cannavò, E., Marian, D., Marín, E. G., Iannaccone, G. & Fiori, G. Transport properties in partially overlapping van der Waals junctions through a multiscale investigation. *Phys. Rev. B* **104**, 085433 (2021).
49. Giannozzi, P. et al. QUANTUM ESPRESSO: a modular and open-source software project for quantum simulations of materials. *J. Phys. Condens Matter* **21**, 395502 (2009).
50. Mostofi, A. A. et al. An updated version of wannier90: a tool for obtaining maximally-localised Wannier functions. *Comput. Phys. Commun.* **185**, 2309–2310 (2014).
51. Liu, Y. et al. Pushing the performance limit of sub-100 nm molybdenum disulfide transistors. *Nano Lett.* **16**, 6337–6342 (2016).


## Acknowledgements

We acknowledge the European Union's Horizon 2020 research and innovation program under the grant agreements QUEFORMAL (829035) and Graphene Flagship (881603), the German Research Foundation (DFG) projects MOSTFLEX (407080863), ULTIMOS$_2$ (LE 2440/8-1) and INST 221/96-1, as well as the German Ministry of Education and Research (BMBF) projects NeuroTec II (16ME0399, 16ME0400) and NeuroSys (03ZU1106xx).

## Author contributions

The manuscript was written through the contributions of all authors. All authors have given approval to the final version of the manuscript.

## Funding

Open Access funding enabled and organized by Projekt DEAL.

## Competing interests

The authors declare no competing interests.

## Additional information

**Supplementary information** The online version contains supplementary material available at https://doi.org/10.1038/s41699-024-00471-y.

**Correspondence** and requests for materials should be addressed to Max C. Lemme.